Structure, Vol. 10, 951–960, July, 2002, ©2002 Elsevier Science Ltd. All rights reserved. PII S0969-2126(02)00788-8

Molecular Mechanism for the Regulation of Human Mitochondrial NAD(P)$^+$-Dependent Malic Enzyme by ATP and Fumarate

Zhiru Yang, Charles W. Lanks, and Liang Tong[1]
Department of Biological Sciences
Columbia University
New York, New York 10027

Summary

The regulation of human mitochondrial NAD(P)$^+$-dependent malic enzyme (m-NAD-ME) by ATP and fumarate may be crucial for the metabolism of glutamine for energy production in rapidly proliferating tissues and tumors. Here we report the crystal structure at 2.2 Å resolution of m-NAD-ME in complex with ATP, Mn^{2+}, tartronate, and fumarate. Our structural, kinetic, and mutagenesis studies reveal unexpectedly that ATP is an active-site inhibitor of the enzyme, despite the presence of an exo binding site. The structure also reveals the allosteric binding site for fumarate in the dimer interface. Mutations in this binding site abolished the activating effects of fumarate. Comparison to the structure in the absence of fumarate indicates a possible molecular mechanism for the allosteric function of this compound.

Introduction

Malic enzyme (ME; EC 1.1.1.40) catalyzes the oxidative decarboxylation of *L*-malate to pyruvate and CO_2, with the concomitant reduction of dinucleotide cofactor NAD^+ or $NADP^+$ [1–5]:

$$NAD(P)^+ + L\text{-malate} \Leftrightarrow NAD(P)H + \text{pyruvate} + CO_2$$

The enzyme also requires the presence of divalent cations (Mg^{2+}, Mn^{2+}, or others) for the catalysis. ME activity was first isolated from pigeon liver and has since been found in most living organisms [6]. The amino acid sequences of malic enzymes are highly conserved, from bacteria to man, consistent with their important biological functions, for example, photosynthesis in plants [7]. Most malic enzymes are homotetramers, with the monomers having about 550 amino acids (60 kDa).

The human mitochondrial NAD(P)$^+$-dependent ME (m-NAD-ME) is believed to play an important role in the metabolism of glutamine for energy production in rapidly proliferating tissues and tumors [8–10]. The activity of this enzyme is regulated by ATP as an inhibitor and by fumarate as an activator [2, 11, 12]. This regulation may be a crucial aspect of the control of this enzyme in glutamine metabolism, as ATP is the ultimate product, and fumarate is the product from the previous step, of the glutamine metabolic pathway. Previous kinetic studies have suggested that both ATP and fumarate act through an allosteric mechanism [9, 12, 13]. However, the molecular basis for this regulation is currently not known.

We recently reported the crystal structures of human m-NAD-ME in both open and closed forms, in complex with NAD^+, Mn^{2+}, and various transition-state analog inhibitors [3, 14–16]. The structures established ME as a new class of oxidative decarboxylases and revealed the binding modes for NAD^+, Mn^{2+}, and the transition-state analogs. The structure of each ME monomer can be divided into four domains (Figure 1A). Domains B (residues 131–277 and 467–538) and C (278–466), together with several residues from domain A, form the active site of the enzyme. The NAD^+ cofactor in the active site is associated with the Rossmann fold of domain C. Domains A (residues 23–130) and D (539–573) are mostly involved in dimer and tetramer formation. The tetramer of the enzyme is a dimer of dimers, with strong interactions at the dimer interface, but weaker interactions at the tetramer interface (Figure 1B). These observations with the human enzyme are confirmed from our structure of the pigeon cytosolic $NADP^+$-dependent malic enzyme (c-NADP-ME) in a closed form, which also reveals the possible molecular mechanism for cofactor selectivity [17].

In the structures of human m-NAD-ME, a second NAD^+ binding site was observed, about 35 Å away from the active site of the enzyme (Figure 1A) [3, 16]. This exo binding site is located near the N-terminal end of the parallel β sheet in domain B, and several residues from domain D also contribute to the formation of this site. The NAD^+ molecule in this exosite is bound using the ADP portion of the cofactor only, and there is specific recognition of the adenine base via hydrogen bonding to its N1 and N6 atoms. Therefore, the structural information appears to suggest that the natural ligand of this exosite may actually be ATP and that this might be the allosteric binding site for ATP in its inhibition of the enzyme [3]. Consistent with this hypothesis, the exosite does not exist in the structure of the pigeon c-NADP-ME, which is not inhibited by ATP [17].

To reveal the molecular basis for the inhibition of human m-NAD-ME by ATP, we have determined the crystal structure of this enzyme in complex with ATP, tartronate, and Mn^{2+}. The structure confirms that ATP is a ligand in the exosite. Somewhat to our surprise, the structure revealed that ATP is also bound in the active site of the enzyme, suggesting that ATP may actually be an active-site inhibitor, rather than an allosteric inhibitor. Our kinetic studies showed that the inhibition by ATP is competitive with NAD^+, consistent with the structural information. To characterize the functional role of the exosite, we carried out structure-based mutagenesis experiments that mutated the three Arg residues important for binding ATP in this site. Our structural and biochemical studies confirmed that the triple mutant can no longer bind ATP in the exosite, but the mutant is still inhibited by ATP. Therefore, our structural, kinetic, and mutagenesis studies demonstrate that ATP is an active-site inhibitor, not an allosteric inhibitor, of human m-NAD-ME.

In order to determine the binding site for the activator fumarate, we have included this compound in previous

[1]Correspondence: tong@como.bio.columbia.edu

Key words: allosteric regulation; energy metabolism; kinetics; protein structure; competitive inhibition; mutagenesis

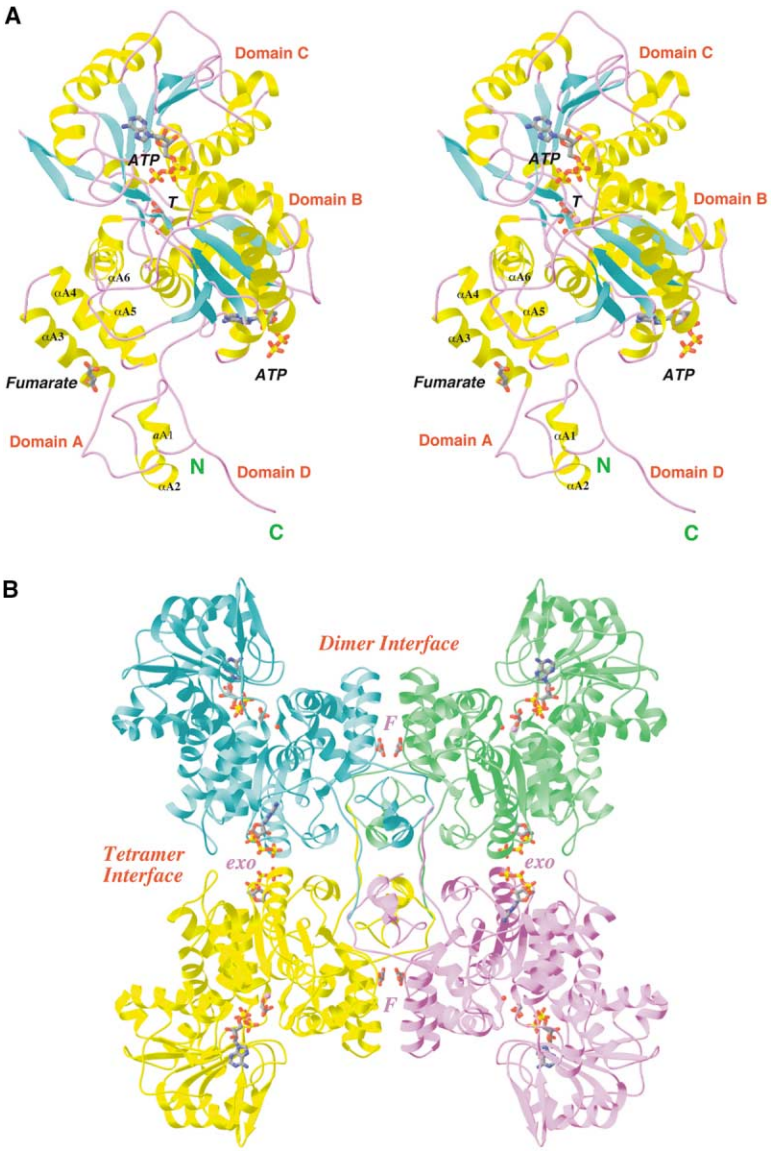

Figure 1. Structure of Human m-NAD-ME in Complex with ATP, Tartronate, Mn^{2+}, and Fumarate

(A) Schematic drawing of the monomer of human m-NAD-ME. β strands, cyan; α helices, yellow; connecting loops, purple. The two ATP molecules, tartronate (labeled *T*), and fumarate are shown as stick models, colored in gray for carbon atoms. The Mn^{2+} ion and its liganding water are shown as pink and red spheres, respectively.

(B) Schematic drawing of the tetramer of the enzyme. The monomers are colored in cyan, green, yellow and purple, respectively. The fumarate molecules are in the dimer interface (labeled *F*). Produced with Ribbons [30].

crystallization experiments but, so far, have not been able to locate it in the electron density map [16]. In the ATP complexes reported here, we were able to observe conclusive evidence for the binding of fumarate to human m-NAD-ME. The binding pocket is located in the dimer interface, about 30 Å from the active site (Figure 1B). Therefore, our structures confirm that fumarate is an allosteric activator of m-NAD-ME. Structure-based mutations in the fumarate binding site abolished the activating effect of this compound. Structural comparisons with the open form of the enzyme, obtained in the absence of fumarate, provide a possible molecular mechanism for the allosteric effects of this compound.

Results

Structure of the ATP Complex

To characterize in detail the interactions between malic enzyme and the ATP inhibitor, we determined the crystal structure of human m-NAD-ME in a "pentary" complex with ATP, Mn^{2+}, tartronate, and fumarate at 2.2 Å resolution (Table 1) (Figure 1A). There is a tetramer of the enzyme in the crystallographic asymmetric unit, and the structures of the four monomers in this tetramer are highly similar to each other (Figure 1B). In addition, the overall structure of the monomer in the ATP complex is essentially the same as that in the NAD^+ complex in the closed form that we reported earlier [14], with rms distance of 0.3 Å for all equivalent Cα atoms. The organization of the tetramer in the ATP complex has only small differences (roughly 0.7° rotation and 0.2 Å translation for each of the monomers) compared to that of the NAD^+ complex. Therefore, our structural analyses show that ATP binding to m-NAD-ME does not cause any significant overall changes in the structure of the monomer or the organization of the tetramer.

In the active site of the enzyme, the binding modes of tartronate and the divalent cation Mn^{2+} are similar to those observed earlier in the NAD^+ complex [14]. There

Table 1. Summary of Crystallographic Information

Enzyme	wild-type	triple mutant
Substrate analog	tartronate	oxalate
Maximum resolution (Å)	2.2	2.3
Number of observations	379,495	250,429
R_{merge} (%)[a]	9.2 (21)	5.0 (8.7)
Resolution range used for refinement	20–2.2	20–2.3
Number of reflections	123,880	119,325
Completeness (%) (2 σ cutoff)	95 (82)	91 (78)
R factor (%)[b]	20.6 (24.4)	19.3 (20.6)
Free R factor (%)	24.2 (27.1)	23.2 (25.4)
Rms deviation in bond lengths (Å)	0.007	0.006
Rms deviation in bond angles (°)	1.3	1.3

[a] $R_{merge} = \sum_h \sum_i |I_{hi} - \langle I_h \rangle| / \sum_h \sum_i I_{hi}$. Numbers in parentheses are for the highest resolution shell.
[b] $R = \sum_h |F_h^o - F_h^c| / \sum_h F_h^o$.

are only small conformational changes for the amino acid residues in the active site, the sole exception being the side chain of Arg165. This residue interacts with the C1 carboxylate group of the inhibitor (or substrate) and the phosphates of the NAD^+ cofactor [3]. In the ATP complex, this side chain has become more disordered, as the conformations of this residue in the four independent monomers are different from each other. This probably reflects a change in the local environment of this residue (see below). Overall, there is little change in the active site of the enzyme in the ATP complex.

ATP Binds in the Exosite as Well as in the Active Site

As expected from structural studies of the NAD^+ complexes, an ATP molecule is bound in the exosite (Figure 2A), showing essentially the same interaction with the enzyme as previously observed for the ADP portion of the NAD^+ cofactor (Figure 2B) [3]. The N6 amino group of the adenine base makes two hydrogen bonds with the main chain carbonyls of residues 192 (3.4 Å) and 556 (2.6 Å), and the N1 ring nitrogen makes a hydrogen bond to the main chain amide of residue 194 (3.0 Å). This hydrogen-bonding pattern provides specific recognition of the adenine base (Figure 2B). The phosphate groups of ATP are on the surface of the structure and interact with a collection of charged side chains, among which the most important are Arg197, Arg542, and Arg556 (Figure 2B). The γ-phosphate of ATP is pointed in the direction of the His154 side chain. The conformation of these residues in the ATP complex is essentially the same as in the NAD^+ complex, with the exception of a 50° rotation in the side chain imidazole ring of the His154 residue (Figure 2B). These structural observations therefore confirm our earlier suggestion that ATP is a natural ligand of this exosite [3].

To our surprise, the structure revealed that ATP is also present in the active site of the enzyme (Figure 3A). Moreover, the conformation of the ADP portion of ATP is remarkably similar to that of the NAD^+ cofactor (Figure 3B). There does not appear to be any specific recognition of the adenine base, as both the N1 and N6 atoms are exposed to the solvent. The γ-phosphate is situated at the opening of the active site pocket (Figure 3C), but this group has much weaker electron density, suggesting that it may be highly disordered (Figure 3A). Residues in the protein that form the ATP binding site generally have the same conformation as in the NAD^+ complex (Figure 3B). The Arg165 side chain becomes more flexible, possibly due to the presence of the additional γ-phosphate. In addition, the Lys345 side chain, which forms one side of the adenine binding pocket

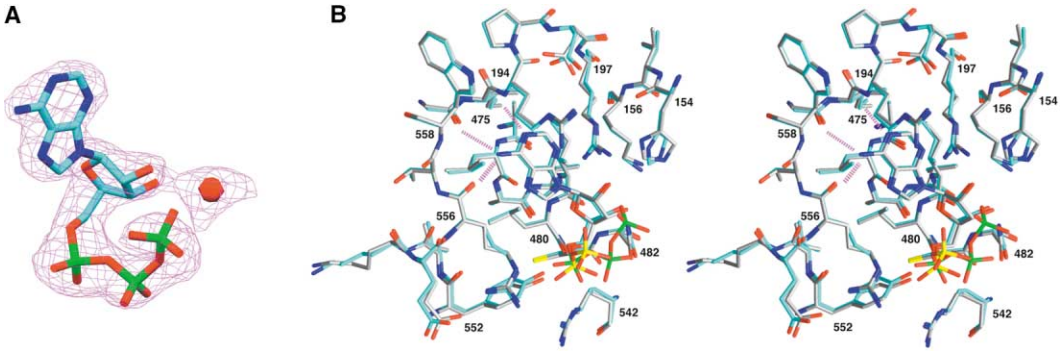

Figure 2. Binding of ATP to the Exosite

(A) Final $2F_o - F_c$ electron density map at 2.3 Å resolution for the ATP molecule in the exosite. The contour level is at 1 σ. Also shown is a water molecule hydrogen bonded to the ribose hydroxyls. Produced with Setor [31].
(B) Stereo diagram showing the binding of ATP to the exosite (in cyan for carbon atoms). For comparison, the binding of the ADP portion of NAD^+ to the exosite (gray) is also shown. Phosphorus atoms of ATP, green; phosphorous atoms of NAD^+, yellow. Produced with Grasp [32].

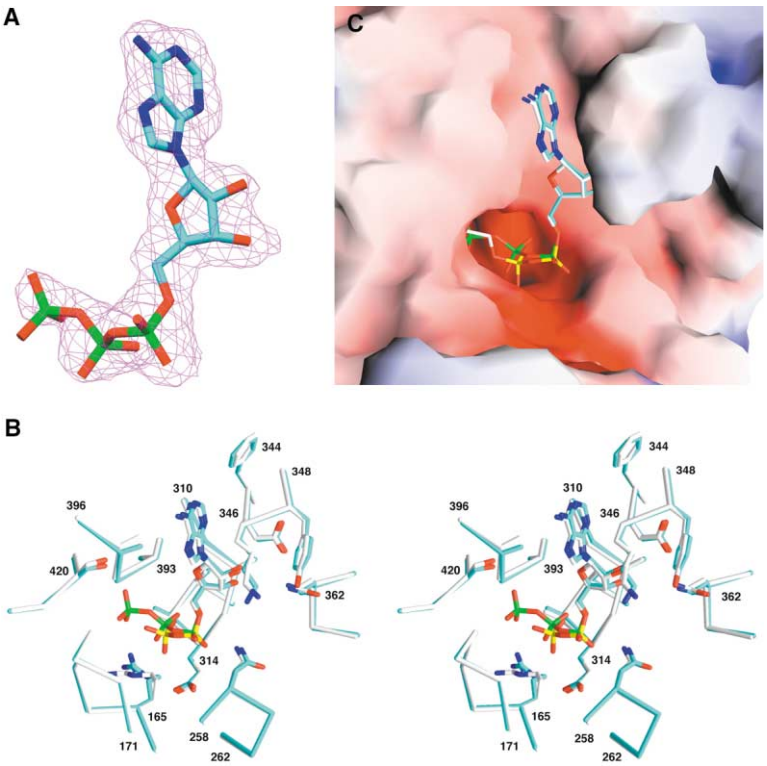

Figure 3. Binding of ATP to the Active Site

(A) Omit $2F_o - F_c$ electron density map at 2.3 Å resolution for the ATP molecule in the active site. The contour level is at 1 σ. Produced with Setor [31].

(B) Stereo diagram showing the binding of ATP to the active site (in cyan for carbon atoms). For comparison, the binding of the ADP portion of NAD^+ to the active site (gray) is also shown.

(C) Molecular surface of human m-NAD-ME in the active site region, colored based on electrostatic potential. The ATP and the NAD^+ molecules are shown in cyan and gray for carbon atoms, respectively. Phosphorus atoms of ATP, green; phosphorous atoms of NAD^+, yellow. Produced with Grasp [32].

(Figure 3B), shows conformational variability among the four monomers in the ATP complex.

Mutagenesis to Disrupt ATP Binding to the Exosite

Based on our structural analyses, residues Arg197, Arg542, and Arg556 may have important roles in the binding of ATP to the exosite (Figure 2B). However, these residues are not conserved among malic enzymes (Figure 4A). Human m-NAD-ME is the only one of the currently known malic enzymes that contains Arg residues at all three positions, and this may be the molecular basis for the unique presence of a binding site in this enzyme.

To dissect the functional role of this exosite in the inhibition by ATP and to verify the importance of the Arg residues for binding ATP, we created mutations that removed the positive charges of the three Arg residues—R197Q, R542V, and R556Q. The mutations were selected based on sequence comparisons between the malic enzymes (Figure 4A). We have prepared and characterized the mutants that carry each of the mutations separately (the single mutants), as well as the triple mutant that carries all three mutations. As expected, the catalytic activity of the mutants is essentially the same as that of the wild-type enzyme (see below and Table 2). It was also clear that the mutants have different biochemical properties. While the R197Q single mutant could be purified using the same protocol as that for the wild-type enzyme, the other two single mutants and the triple mutant could not, as they no longer bind to the ATP affinity column. This suggests that ATP binding to the exosite may have been disrupted by these mutations. Moreover, the results demonstrate that binding to the ATP affinity resin is mediated by the exosite, in contrast to earlier suggestions that the binding is mediated by the active site [9].

To confirm that ATP binding to the exosite of the triple mutant was disrupted, we determined the crystal structure of the triple mutant in complex with ATP, oxalate, and Mn^{2+} at 2.3 Å resolution (Table 1). The overall structure of the monomer of the mutant is similar to that of the wild-type, with rms distance of 0.4 Å for all equivalent Cα atoms. As with the wild-type enzyme, an ATP molecule is observed in the active site of the structure, having essentially the same conformation and interactions with the enzyme (data not shown). The binding modes of Mn^{2+} and oxalate are also the same as that observed for the wild-type enzyme.

However, we did not observe the presence of ATP in the exosite (Figure 4B), therefore confirming that the three Arg residues are crucial for ATP binding. The three mutations introduced a significant change in the electrostatic surface potential of the exopocket (Figures 4C and 4D), which may be the principal reason for the lack of ATP binding by the triple mutant. In addition, the mutations introduced steric clashes between the adenine base and the enzyme (Figures 4B and 4D).

There is also a change in the organization of the tetramer of the triple mutant, equivalent to rotations of about 1.7° and translations of about 0.2 Å for each of the monomers. The observed differences are more likely due to the mutations themselves than to the lack of ATP binding to the exosite. Of the three mutations, R542V is located in the tetramer interface; therefore, it may have a direct impact on the organization of the tetramer. However, the catalytic activity of the triple mutant is essentially not affected (Table 2).

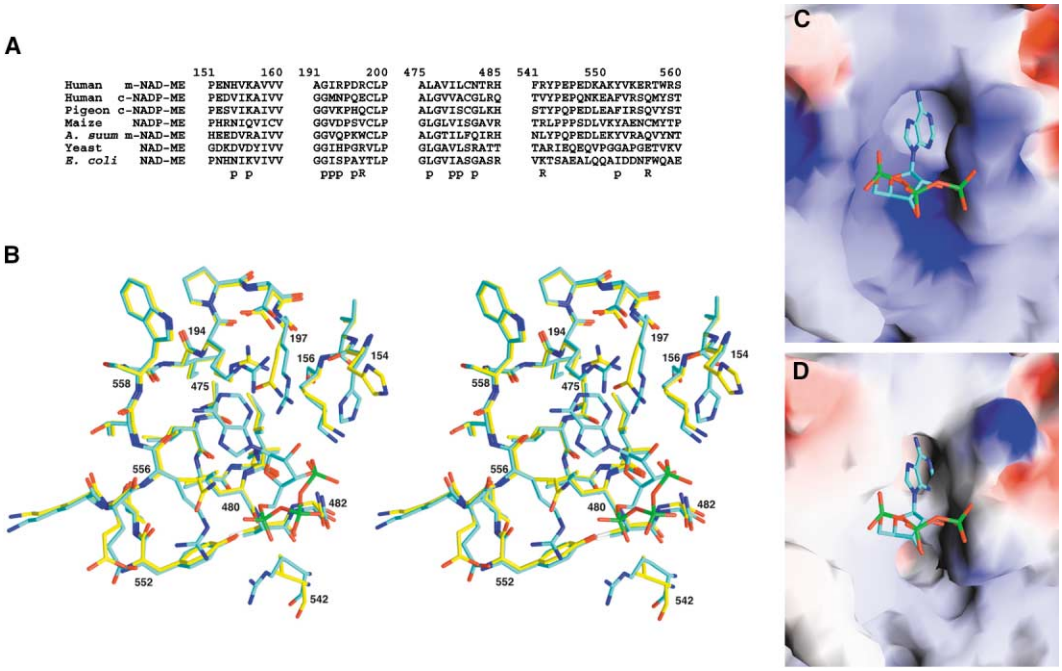

Figure 4. The Exosite Is Removed by Structure-Based Mutations

(A) Sequence alignment of residues in the exo binding site. p, residues that interact with ATP; R, mutated Arg residues.

(B) Stereo diagram showing the exopocket in the triple mutant (in yellow for carbon atoms). For comparison, the binding of ATP to the wild-type enzyme (cyan) is also shown.

(C) Molecular surface of the exosite in the wild-type enzyme. The ATP molecule is shown as a stick model.

(D) Molecular surface of the exosite in the triple mutant. The ATP molecule in the wild-type complex is shown for reference. Note the steric clash between ATP and the mutant enzyme and the change in the electrostatic surface features. Produced with Grasp [32].

ATP Is a Competitive Inhibitor with Respect to NAD^+

Our structural studies of wild-type human m-NAD-ME revealed ATP binding to both the active site and the exosite, thus raising the question as to which of the two sites, or maybe both of them, contributes to the inhibition by ATP. This prompted us to characterize in detail the kinetics of inhibition by ATP. Our kinetic results showed that ATP is a competitive inhibitor of wild-type m-NAD-ME with respect to NAD^+ (Figure 5), with a K_i of about 0.2 mM (Table 2), consistent with earlier results [9, 18]. This suggests that ATP binding in the active site may be inhibitory, as it would compete with NAD^+ for the enzyme.

To study the kinetic effects of ATP binding to the exopocket, we next characterized the ATP inhibition of the triple mutant. Our structural studies confirmed that the exosite can no longer bind ATP in this mutant (Figure 4D), and ATP, therefore, can only bind in the active site. The kinetic studies showed that the triple mutant has roughly the same catalytic activity as the wild-type enzyme. More importantly, the pattern of ATP inhibition of the triple mutant is essentially identical to that of the wild-type enzyme, also with a K_i of 0.2 mM (Table 2). This demonstrates that the inhibition by ATP occurs solely through binding at the active site. ATP binding to the exosite does not produce any recognizable effects on the catalysis by this enzyme. Kinetic studies with single mutants (R197Q and R542V) produced similar results to those of the triple mutant (Table 2). Therefore, contrary to prior expectations, ATP is not an allosteric inhibitor, but, rather, an active site inhibitor of human m-NAD-ME.

Our structures show that only the ADP portion of the ATP molecule in the active site is highly ordered in the complex (Figure 3A), suggesting that ADP should also be able to inhibit the enzyme. Our kinetic experiments confirm that ADP is a competitive inhibitor of m-NAD-

Table 2. Kinetic Parameters for the Inhibition by ATP and ADP of m-NAD-ME

Enzyme	Inhibitor	K_m (μM)[a]	V_{max} ($\times 10^{-3}$ AU/s)[b]	K_i (mM)
Wild-type	ATP	93 ± 10	4.1 ± 0.2	0.20 ± 0.02
Wild-type	ADP	150 ± 14	7.0 ± 0.3	0.99 ± 0.08
R197Q	ATP	230 ± 18	7.1 ± 0.3	0.58 ± 0.06
R542V	ATP	294 ± 41	4.1 ± 0.4	0.79 ± 0.15
Triple mutant	ATP	295 ± 26	2.6 ± 0.2	0.20 ± 0.01

[a] Value for NAD^+ in the absence of the inhibitor.

[b] Value for same concentration of various enzymes. AU, absorbance unit.

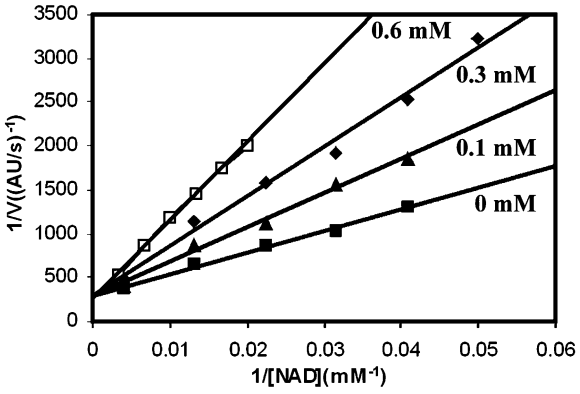

Figure 5. ATP Is a Competitive Inhibitor of NAD^+

Lineweaver-Burk (double-reciprocal) plots for different concentrations of ATP illustrate the competitive behavior of the inhibition. The kinetic parameters were obtained by least-squares fitting to data at all ATP concentrations simultaneously [29].

ME with respect to NAD^+, with an equivalent K_i of 1 mM (Table 2).

To determine the nucleotide specificity of this inhibition, we assayed the inhibitory effects of several other nucleotides on human m-NAD-ME. The results showed that GTP has an inhibitory effect on this enzyme that is comparable to that of ADP (our own unpublished data). This is consistent with our structural observations, as there is no specific recognition of the adenine base in the active site. Moreover, it is unlikely that GTP can bind in the exosite, due to the specific recognition of adenine by that pocket. This again confirms that the inhibition by ATP and GTP occurs through the active site. On the other hand, CTP and TTP have no inhibitory effects on this enzyme, suggesting that binding in the active site may require purine nucleotides.

In comparison, the nucleotides ATP, ADP, and GTP have no inhibitory effects on the pigeon c-NADP-ME (data not shown). This is likely due to the lack of the 2′-phosphate group on the ribose of these nucleotides, as the natural cofactor for this enzyme is $NADP^+$. The 2′-phosphate is recognized in part by the side chain of Lys362 in the pigeon enzyme (Figure 3B) [17, 19]. On the other hand, the malic enzyme from *Ascaris suum* uses NAD^+ as the cofactor but is not inhibited by ATP [20]. There may be additional factors that determine the binding affinity for ATP in the active site.

Binding Site for the Activator Fumarate

To locate the binding site of the activator fumarate, we included this compound at 5 mM concentration in our crystallization experiments for the NAD^+ complexes but could not observe conclusive evidence for the binding of this compound [14]. Unexpectedly, we observed clear electron density for fumarate in the ATP complexes reported here (Figure 6A).

Fumarate is bound at the dimer interface (Figure 1B), about 30 Å away from the active site, confirming that fumarate functions through an allosteric mechanism. It is docked in a pocket on the surface of domain A of one monomer (Figure 1A). Residues from helices αA3 and αA4, together with residues in the αA1-αA2 linker, form this binding pocket (Figure 6B). One carboxylate group of fumarate shows bidentate ion pair interactions with the side chain of Arg91, and the other carboxylate forms a monodentate ion pair with Arg67. At the dimer interface, residues 123–130 from the other monomer, in the linker between domain A and domain B, cover the fumarate molecule (Figure 6B), which helps to shield this binding site from the solvent (Figure 6C). This pocket is highly hydrophilic in nature. There are more than five solvent water molecules in the pocket, bridging the interactions between fumarate and the protein.

Both Arg67 and Arg91 are well conserved among the plant and animal malic enzymes (Figure 7A). To confirm the structural observations on this binding site, we made the R67S and R91T single-point mutants, based on the sequence comparisons (Figure 7A). We also generated the E59L mutant. This residue is ion paired with Arg67 in the structure (Figure 6B) but is not conserved among the malic enzymes (Figure 7A). Our kinetic studies showed that the wild-type enzyme is activated by about 2-fold by the presence of 5 mM fumarate and saturating concentrations of the substrates, whereas neither of the three mutants is affected by the presence of fumarate (Figure 7B). Under physiological conditions, with subsaturating amounts of the substrates, the effects of fumarate on the enzyme activity can be much greater, more than 20-fold based on our preliminary measurements (data not shown). This clearly demonstrates the biological relevance of the fumarate binding pocket observed in our structures. Our data also explain why pigeon malic enzyme is not activated by fumarate, as it contains a Ser residue at position 67 (Figure 7A). At the same time, it is interesting to note that the malic enzyme from *Ascaris suum* is activated by fumarate [20], which has Arg residues at both 67 and 91, although with a Met residue at 59 (Figure 7A).

With the knowledge of the fumarate binding site, we reexamined the electron density maps of our earlier NAD^+ complexes, which were produced in the presence of 5 mM fumarate [14]. Crystals of the NAD^+ and the ATP complexes are actually isomorphous with each other. There was clear electron density at the two carboxylate positions of fumarate in the earlier electron density maps, but the two pieces of density are not connected. Nonetheless, residues that form this binding site in the NAD^+:Mn^{2+}:oxalate quaternary complex have the same conformation as the current ATP:Mn^{2+}:tartronate:fumarate pentary complex. Moreover, the positions of the solvent molecules in this pocket in the NAD^+ complex are also similar to those observed here in the ATP complex. Therefore, it is likely that fumarate may also be bound in the earlier NAD^+ complexes, although it might have been more disordered.

Discussion

The regulation of human m-NAD-ME by ATP and fumarate is consistent with the role of human m-NAD-ME in the metabolism of glutamine for energy production [8, 9] and is reminiscent of the regulation of pyruvate kinase in the glycolysis pathway [3]. The inhibition by ATP rep-

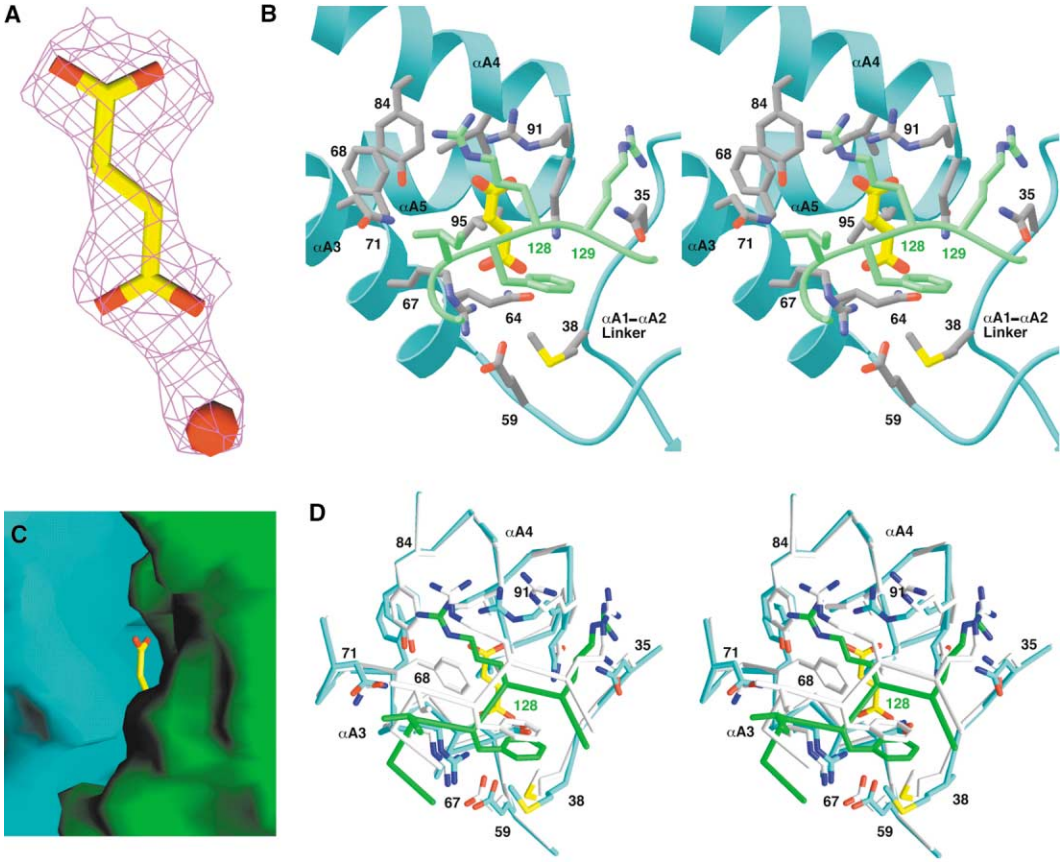

Figure 6. The Fumarate Binding Site

(A) Final $2F_o - F_c$ electron density map at 2.3 Å resolution for fumarate, together with a water molecule. The contour level is at 1 σ. Produced with Setor [31].

(B) Stereo diagram showing the binding of fumarate (in yellow for carbon atoms) to the allosteric site (in cyan and green for the two monomers).

(C) Molecular surface of m-NAD-ME dimer near the fumarate binding site (cyan and green). The fumarate molecule is mostly shielded from the solvent.

(D) Stereo diagram showing the lack of the fumarate binding site in the open form of the enzyme (in gray for carbon atoms) [3]. The fumarate complex in the closed form is shown in cyan and green for the two monomers. The change in the dimer organization can be recognized by the poor fit of the second monomer (green). Produced with Grasp [32].

resents feedback control on this metabolic pathway. Our kinetic analyses showed that the K_i of ATP is around 0.2 mM, suggesting that the enzyme will be mostly inactive under normal physiological conditions, with a mitochondrial ATP concentration of about 2 mM. As the mitochondrial concentration of ADP is generally much lower, the inhibition of this enzyme by ADP is unlikely to be physiologically relevant.

To determine the molecular mechanism of the inhibition of m-NAD-ME by ATP, we determined the crystal structure of the enzyme in complex with the inhibitor. It revealed the binding of ATP to both the active site and an exosite. To dissect the functional roles of the two binding sites in the inhibition, we introduced structure-based mutations in the exosite, and our structural analysis confirmed that the exosite has been "knocked out" in the R197Q, R542V, and R556Q triple mutant. Kinetic studies showed that this triple mutant is inhibited by ATP at essentially the same level as the wild-type enzyme and that the inhibition is competitive relative to NAD^+. These data provide conclusive evidence that the inhibition by ATP occurs via the active site, in contrast to earlier expectations that ATP is an allosteric inhibitor of the enzyme [9, 13]. Therefore, ATP inhibits human m-NAD-ME by competing with NAD^+ for binding to the active site of the enzyme.

The binding of ATP to the active site is somewhat surprising, as the pocket is highly exposed to the solvent (Figure 3C). This may be consistent with the relatively low affinity of this pocket for ATP, with K_i in the millimolar range. In contrast, NAD^+ is bound to this site with the nicotinamide ring completely shielded from the solvent, and the affinity of the active site for the dinucleotide cofactor is in the micromolar range [21].

Our biochemical data suggest that the R197Q single mutant may still be able to bind ATP in the exosite, as it can still bind to the ATP affinity column. In contrast, the R542V and R556Q single mutants and the triple mutant no longer bind the ATP affinity resin. This suggests that R542 and R556 may have a larger contribution to the binding of ATP in the exosite, which appears to be consistent with our structural information. The R197 side

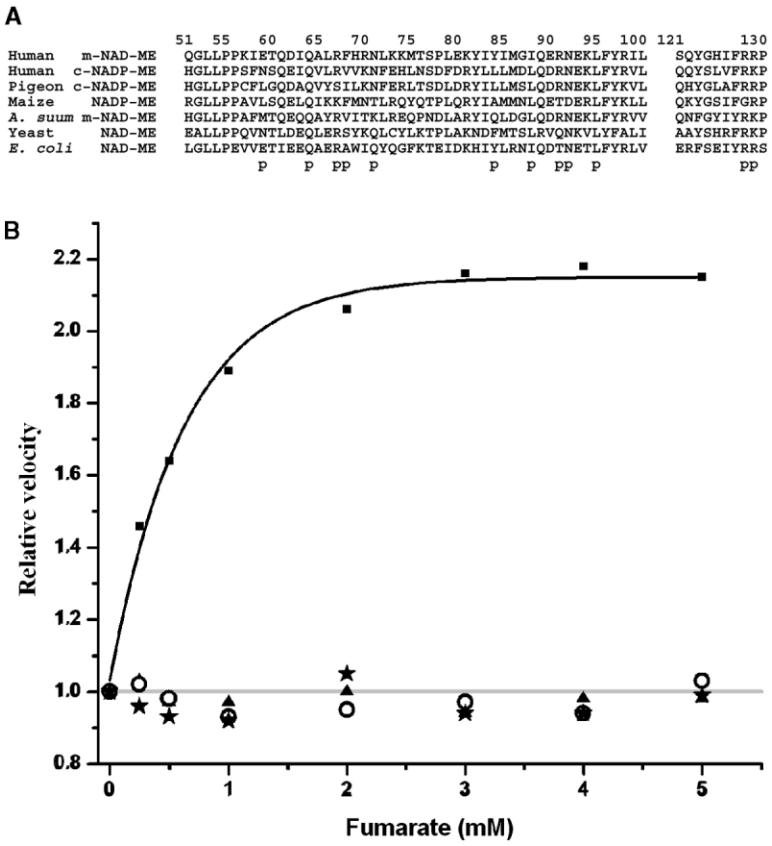

Figure 7. Structure-Based Mutations Abolish the Allosteric Effects of Fumarate

(A) Sequence alignment of residues in the fumarate binding site. p, residues that interact with fumarate.

(B) Effects of fumarate on the catalytic activity of wild-type (squares) and the R67S (circles), R91T (stars), and E59L (triangles) mutants of m-NAD-ME. For each enzyme, the initial velocity of the reaction in the absence of fumarate is set at 1. The activity of the mutants is not affected by fumarate.

chain is further away from the α- and β-phosphates of ATP (Figure 2B).

The binding of ATP to the exosite has little impact on the catalysis by the enzyme. Further studies will be needed to determine whether this binding has any other functional or structural impacts on the enzyme. It may be possible that binding of ATP in the exopocket helps to stabilize human m-NAD-ME under physiological conditions.

Fumarate is the product of the previous step of the pathway in the metabolism of glutamine for energy production [8]. Its activation of m-NAD-ME may help ensure that there is enough ME activity when the pathway is functional. Our studies confirm that fumarate has an allosteric binding pocket. Arg67 and Arg91 are two important residues in fumarate binding, and their mutation can abolish the effects of this compound. Surprisingly, these residues are conserved in many of the plant and animal malic enzymes (Figure 7A), suggesting that there may be additional factors that control the binding of fumarate to malic enzymes.

Our first structure of m-NAD-ME, in a binary complex with NAD^+, was obtained in the absence of fumarate [3]. The fumarate binding pocket does not exist in this open form structure. The side chain of Phe68 assumes a different rotamer and blocks the binding site, and the side chain guanidinium group of Arg91 is rotated away from the binding site (Figure 6D). A major component of the conformational differences between the open and closed forms of the enzyme is the change in the dimer and tetramer interface (Figure 6D) [14]. The fumarate binding pocket is in the dimer interface, and both Arg91 and Arg129 are located next to the 2-fold axis of the dimer. It is possible that fumarate promotes the reorganization of the enzyme tetramer, and this may be the molecular mechanism for its allosteric effects on the catalysis by human m-NAD-ME.

Biological Implications

Malic enzymes catalyze the oxidative decarboxylation of malate to produce pyruvate and CO_2, together with the reduction of the $NAD(P)^+$ cofactor. They are widely distributed in nature and have important biological functions, such as photosynthesis in plants and fatty acid biosynthesis in animals. The human mitochondrial $NAD(P)^+$-dependent malic enzyme (m-NAD-ME) is believed to participate in the metabolism of glutamine for the production of energy in rapidly proliferating tissues and tumors. This enzyme is regulated by ATP as an inhibitor and by fumarate as an activator. This regulation is consistent with the functional role of this enzyme, as ATP is the overall product of energy metabolism and fumarate is from the previous step in the metabolic pathway. This regulation parallels that of pyruvate kinase in the glycolysis pathway.

Our studies here showed that ATP is an active site inhibitor of the enzyme, even though there is an exo binding site for this molecule on the enzyme. This exo binding site appears to be unique to this enzyme, and its exact biological roles (if any) remain unknown. Mutations in the exosite can abolish the binding of ATP but

have little impact on the catalytic activity of the enzyme. Under normal physiological conditions, it is likely that this enzyme is strongly inhibited by ATP, as its K_i is about 0.2 mM.

We have also observed the binding of fumarate to the enzyme. The binding site is located at the dimer interface, far from the active site of the enzyme. This confirms earlier kinetic studies suggesting that fumarate is an allosteric activator. Mutations of residues in this binding pocket can desensitize the enzyme toward fumarate, confirming the structural observations. Under physiological conditions, fumarate may be able to activate the enzyme by more than 20-fold. Our structural studies suggest that fumarate may induce a change in the organization of the tetramer of the enzyme and that this conformational change may be the molecular mechanism for its allosteric activating effects.

Experimental Procedures

Protein Expression, Purification, and Crystallization

The protocols for the expression and purification of wild-type human m-NAD-ME have been described previously [2, 22]. Briefly, m-NAD-ME was cloned in the pRH281 vector, overexpressed in *E. coli*, and purified by anion exchange, ATP affinity, and gel filtration chromatography. The site-specific mutants of human m-NAD-ME (R197Q, R542V, R556Q, R67S, R91T, and E59L) were prepared with the QuikChange kit (Stratagene) and sequenced to confirm the presence of the mutations. As some of these mutants can no longer bind the ATP affinity resin, we introduced a His_6 tag at the C terminus of the wild-type enzyme in the pRH281 vector. With this tag, the enzymes were purified by Ni-NTA affinity, anion exchange, and gel filtration chromatography. The catalytic activity of this His-tagged wild-type m-NAD-ME is essentially the same as that of the untagged enzyme, confirming that the introduction of the affinity tag did not affect the function of the protein. This is consistent with the structural information, as the C-terminal 11 residues of the enzyme are not observed in the crystal structures.

Crystals of both untagged wild-type and His-tagged mutant human m-NAD-ME were obtained at 4°C by the hanging-drop vapor diffusion method. The protein was at 8 mg/ml concentration, in a buffer containing 30 mM Tris (pH 7.4), 70 mM KCl, 10 mM ATP, 5 mM fumarate, 5 mM $MnCl_2$, 2 mM DTT, and 5 mM tartronate or oxalate. The reservoir solution contained 100 mM MES (pH 6.0), 8%–10% (w/v) PEG 20,000, and 5% (v/v) MPD. Crystals in the shape of thin plates appeared within two days. The crystals were transferred to a cryoprotection solution containing 100 mM MES (pH 6.0), 35% (w/v) PEG 8000, 5% MPD (v/v), and 5 mM fumarate and flash frozen in liquid propane for X-ray analysis.

Data Collection and Processing

X-ray diffraction data at 2.2 Å resolution on the wild-type m-NAD-ME in complex with ATP and tatronate were collected at beamline 32-ID (ComCAT) at the Advanced Photon Source (APS). The diffraction images were recorded on a Mar CCD and processed with the HKL package [23]. The crystals belong to space group C2, with cell parameters of a = 224.9 Å, b = 117.4 Å, c = 111.6 Å, and β = 109.3°. The data processing statistics are summarized in Table 1.

X-ray diffraction data to 2.3 Å resolution for the triple mutant were collected at beamline X8C at the National Synchrotron Light Source (NSLS). The diffraction images were recorded on an ADSC Quantum-4 CCD and processed with the HKL package [23]. The crystal belongs to space group $P2_1$, with cell parameters of a = 71.8 Å, b = 192.6 Å, c = 110.2 Å, and β = 89.8°, with a tetramer in the asymmetric unit (Table 1).

Structure Determination and Refinement

The crystals of wild-type m-NAD-ME in complex with ATP are isomorphous to those in complex with NAD^+ in the close form that we reported earlier [14], with a tetramer in the asymmetric unit. The structure refinement was carried out with the program CNS [24], and the atomic model was rebuilt against the $2F_o - F_c$ electron density maps with the program O [25]. After initial refinement with the protein atoms only, the resulting electron density map clearly showed the binding of Mn^{2+}, ATP, and tartronate in the active site, as well as the binding of ATP in the exosite. The refinement statistics are summarized in Table 1.

The structure of the triple mutant was determined by the combined molecular replacement protocol, with the program COMO [26, 27]. The structure of m-NAD-ME in a closed form was used as the search model [14]. Reflection data between 10 and 4 Å resolution were used in the calculation. The atomic model from the molecular replacement solution was subjected to rigid body refinement against reflection data between 5 and 4 Å resolution with CNS [24]. Calculated phases based on this atomic model (protein atoms only) were applied to all the observed reflections between 20 and 2.5 Å resolution, and the phase information was improved by 4-fold noncrystallographic symmetry (NCS) averaging, with the program DM [28]. The atomic model was rebuilt against this electron density map, which also revealed the binding of ATP, Mn^{2+}, and oxalate in the active site. There is no electron density for an ATP molecule in the exosite. NCS restraints on the main chain atoms were used during the crystallographic refinement. The refinement statistics are summarized in Table 1.

Kinetic Assays

The m-NAD-ME reaction buffer contained 50 mM triethanolamine-HCl (pH 7.4), 10 mM $MgCl_2$, 10 mM *L*-malate, 5 mM fumarate, and 0.3 mM NAD^+. The reaction was started by the addition of enzyme, and the reaction velocity was determined by following A_{340} (absorption of NADH) for 5 min. To minimize errors in the absorbance measurements, a 5 cm path-length cuvette was used in all the kinetic assays.

The inhibitory effect of ATP was assayed on the wild-type m-NAD-ME, the R197Q and R542V single mutants, and the triple mutant. His-tagged proteins were used in the assays, and the protein concentrations were determined by the Bradford method. The NAD^+ concentration was varied between 20 and 250 μM, and ATP concentration was varied from 0 to 0.6 mM. To avoid the depletion of Mg^{2+} by ATP, a 1:1 mixture of Mg^{2+}:ATP was used. The observed kinetic data showed a fully competitive pattern, and the kinetic parameters were obtained by least-squares fitting against data at all ATP concentrations [29].

The inhibitory effect of ADP was assayed following the same protocol, and the ADP concentration was varied between 0 and 1.5 mM. The inhibitory effects of other nucleotides (GTP, CTP, and TTP) were also examined.

The activating effect of fumarate was assayed using reaction buffers with varying amounts of fumarate (between 0 and 5 mM). The initial velocities of the reactions were determined.

Acknowledgments

We thank Dr. W.W. Cleland for help with the fitting of our kinetic data and for valuable discussions, Hailong Zhang for help with the crystallographic analysis, Sozanne Solmaz for characterizing the inhibition of the enzyme by other nucleotides, Reza Khayat, Yingwu Xu, Renu Batra, Gerwald Jogl, and Xiao Tao for help with data collection at the synchrotrons, Joel Berendzen for access to the X8C beamline at NSLS, and Steve Wasserman and Kevin D'Amico for access to the 32-ID beamline at APS. This work was supported by the National Science Foundation (grant number MCB-99-74700 to L.T.).

Received: February 26, 2002
Revised: April 18, 2002
Accepted: April 19, 2002

References

1. Hsu, R.Y., and Lardy, H.A. (1967). Pigeon liver malic enzyme. II. Isolation, crystallization, and some properties. J. Biol. Chem. *242*, 520–526.

2. Loeber, G., Infante, A.A., Maurer-Fogy, I., Krystek, E., and Dworkin, M.B. (1991). Human NAD$^+$-dependent mitochondrial malic enzyme. J. Biol. Chem. *266*, 3016–3021.
3. Xu, Y., Bhargava, G., Wu, H., Loeber, G., and Tong, L. (1999). Crystal structure of human mitochondrial NAD(P)+-dependent malic enzyme: a new class of oxidative decarboxylases. Structure *7*, 877–889.
4. Rao, G.S.J., Coleman, D.E., Kulkarni, G., Goldsmith, E.J., Cook, P.F., and Harris, B.G. (2000). NAD-malic enzyme from Ascaris suum: sequence and structural studies. Protein. Pept. Lett. *7*, 297–304.
5. Cleland, W.W. (2000). Chemical mechanism of malic enzyme as determined by isotope effects and alternate substrates. Prot. Peptide Lett. *7*, 305–312.
6. Ochoa, S., Mehler, A., and Kornberg, A. (1947). Reversible oxidative decarboxylation of malic acid. J. Biol. Chem. *167*, 871–872.
7. Hibberd, J.M., and Quick, W.P. (2002). Characteristics of C4 photosynthesis in stems and petioles of C3 flowering plants. Nature *415*, 451–454.
8. McKeehan, W.L. (1982). Glycolysis, glutaminolysis and cell proliferation. Cell Biol. Int. Rep. *6*, 635–650.
9. Moreadith, R.W., and Lehninger, A.L. (1984). Purification, kinetic behavior, and regulation of NAD(P)$^+$ malic enzyme of tumor mitochondria. J. Biol. Chem. *259*, 6222–6227.
10. Baggetto, L.G. (1992). Deviant energetic metabolism of glycolytic cancer cells. Biochimie *74*, 959–974.
11. Frenkel, R. (1972). Allosteric characteristics of bovine heart mitochondrial malic enzyme. Biochem. Biophys. Res. Commun. *47*, 931–937.
12. Sauer, L.A. (1973). An NAD- and NADP-dependent malic enzyme with regulatory properties. Biochem. Biophys. Res. Commun. *50*, 524–531.
13. Zdnierowicz, S., Swierczynski, J., and Selewski, L. (1988). Purification and properties of the NAD(P)+-dependent malic enzyme from human placental mitochondria. Biochem. Med. Metab. Biol. *39*, 208–216.
14. Yang, Z., Floyd, D.L., Loeber, G., and Tong, L. (2000). Structure of a closed form of human malic enzyme and implications for catalytic mechanism. Nat. Struct. Biol. *7*, 251–257.
15. Yang, Z., Batra, R., Floyd, D.L., Hung, H.-C., Chang, C.-G., and Tong, L. (2000). Potent and competitive inhibition of malic enzymes by lanthanide ions. Biochem. Biophys. Res. Commun. *270*, 440–444.
16. Yang, Z., and Tong, L. (2000). Structural studies of a human malic enzyme. Protein Pept. Lett. *7*, 287–296.
17. Yang, Z., Zhang, H., Hung, H.-C., Kuo, C.-C., Tsai, L.-C., Yuan, H.S., Chou, W.-Y., Chang, G.-G., and Tong, L. (2002). Structural studies of pigeon cytosolic NADP+-dependent malic enzyme. Protein Sci. *11*, 332–341.
18. Mandella, R.D., and Sauer, L.A. (1975). The mitochondrial malic enzymes. J. Biol. Chem. *250*, 5877–5884.
19. Kuo, C.-C., Tsai, L.-C., Chin, T.-Y., Chang, G.-G., and Chou, W.-Y. (2000). Lysine residues 162 and 340 are involved in the catalysis and coenzyme binding of NADP+-dependent malic enzyme from pigeon. Biochem. Biophys. Res. Commun. *270*, 821–825.
20. Landsperger, W.J., and Harris, B.G. (1976). NAD+-malic enzyme. Regulatory properties of the enzyme from Ascaris suum. J. Biol. Chem. *251*, 3599–3602.
21. Satterlee, J., and Hsu, R.Y. (1991). Duck liver malic enzyme: sequence of a tryptic peptide containing the cysteine residue labeled by the substrate analog bromopyruvate. Biochim. Biophys. Acta *1079*, 247–252.
22. Bhargava, G., Mui, S., Pav, S., Wu, H., Loeber, G., and Tong, L. (1999). Preliminary crystallographic studies of human mitochondrial NAD(P)$^+$-dependent malic enzyme. J. Struct. Biol. *127*, 72–75.
23. Otwinowski, Z., and Minor, W. (1997). Processing of X-ray diffraction data collected in oscillation mode. Methods Enzymol. *276*, 307–326.
24. Brunger, A.T., Adams, P.D., Clore, G.M., DeLano, W.L., Gros, P., Grosse-Kunstleve, R.W., Jiang, J.-S., Kuszewski, J., Nilges, M., Pannu, N.S., et al. (1998). Crystallography and NMR System: a new software suite for macromolecular structure determination. Acta Crystallogr. D Biol. Crystallogr. *54*, 905–921.
25. Jones, T.A., Zou, J.Y., Cowan, S.W., and Kjeldgaard, M. (1991). Improved methods for building protein models in electron density maps and the location of errors in these models. Acta Crystallogr. A *47*, 110–119.
26. Tong, L. (1996). Combined molecular replacement. Acta Crystallogr. A *52*, 782–784.
27. Jogl, G., Tao, X., Xu, Y., and Tong, L. (2001). COMO: a program for combined molecular replacement. Acta Crystallogr. D Biol. Crystallogr. *57*, 1127–1134.
28. CCP4 (Collaborative Computational Project 4) (1994). The CCP4 suite: programs for protein crystallography. Acta Cryst. D Biol. Crystallogr. *50*, 760–763.
29. Cleland, W.W. (1979). Statistical analysis of enzyme kinetic data. Methods Enzymol. *63*, 103–138.
30. Carson, M. (1987). Ribbon models of macromolecules. J. Mol. Graph. *5*, 103–106.
31. Evans, S.V. (1993). SETOR: hardware lighted three-dimensional solid model representations of macromolecules. J. Mol. Graph. *11*, 134–138.
32. Nicholls, A., Sharp, K.A., and Honig, B. (1991). Protein folding and association: insights from the interfacial and thermodynamic properties of hydrocarbons. Proteins *11*, 281–296.

Accession Numbers

The atomic coordinates have been deposited with the Protein Data Bank under entry codes 1gz3 and 1gz4.